Self-stresses and crack formation by particle swelling in cohesive granular media

M. S. El Youssoufi, J.-Y. Delenne, and F. Radjai
LMGC, CNRS-Université Montpellier II, Place Eugène Bataillon, 34095 Montpellier Cedex, France
(Received 12 July 2004; revised manuscript received 31 March 2005; published 27 May 2005)

We present a molecular-dynamics study of force patterns, tensile strength, and crack formation in a cohesive granular model where the particles are subjected to swelling or shrinkage gradients. Nonuniform particle size change generates self-equilibrated forces that lead to crack initiation as soon as the strongest tensile contacts begin to fail. We find that the tensile strength is well below the theoretical strength as a result of inhomogeneous force transmission in granular media. The cracks propagate either inward from the edge upon shrinkage or outward from the center upon swelling. We show that the coarse-grained stresses are correctly predicted by an elastic model that incorporates particle size change as metric evolution.

DOI: 10.1103/PhysRevE.71.051307 PACS number(s): 83.80.Fg, 45.70.Mg, 81.05.Rm

The term "cohesive granular media" covers a vast spectrum of granular materials in which rigid grains are bound together by cohesion forces of various chemico-physical origins [1]. Well-known examples are fine powders and soils with more or less colloidal or water content [2]. The solidlike behavior attributed to noncohesive granular media under quasistatic shearing becomes the dominant feature in the presence of cohesion, with an increasing effective tensile strength as a function of the contact tensile strength [3–6]. The stress-strain behavior and fracture mechanics of cohesive granular media raise interesting open issues from a grain-scale point of view and in interaction with heat or mass transfer [6–11].

An appealing issue is how and in which respects these "granular solids" differ from molecular solids (in the absence of a granular structure) [12]. For example, the phenomenon of stress concentration, induced by defects at different scales, governs the initiation of failure in molecular solids, the effective tensile strength remaining generally far below the "theoretical" strength [13]. In a granular assembly, stress concentration occurs already at the particle scale in the form of a highly inhomogeneous distribution of contact forces [14,15]. This suggests that, even in the absence of mesoscopic defects, the tensile strength will be weak compared to its theoretical value for a granular assembly (to be defined below). However, the tensile-strength properties have scarcely been analyzed from a microscopic standpoint.

In this paper, we consider a benchmark test that was designed to probe the *intrinsic* tensile response (reflecting only the granular disorder) of a cohesive granular sample by avoiding both wall effects and strain localization as spurious sources of randomness. The sample consists of rigid cohesive disks compacted numerically into a circular form in a two-dimensional space; see Fig. 1(a). At the start, the normal force is exactly zero at all contacts. Then, the particle diameters are increased (or decreased) at a rate that depends on distance to the sample center. Such gradients of particle size change occur, for instance, in fine soils, where particle swelling (or shrinkage) happens as a result of humidification (or drying) [2]. As we shall see in detail below, this bulk straining induces a field of radial (or orthoradial) tensile self-stresses increasing in magnitude with time, and leading eventually to crack initiation at the center (or on the edge).

For the simulations, we used the molecular-dynamics method with a velocity-Verlet scheme for the integration of the equations of motion [16]. Cohesive interaction between two particles implies resistance to relative motion (normal displacement d_n, tangential displacement d_t, and angular displacement γ) of two edge points belonging, respectively, to the two particles and coinciding initially with the contact point; see Fig. 1(b). The corresponding contact actions are the normal force f_n, the tangential force f_t, and the contact torque M. Several force-displacement relations have been proposed in order to model cohesive contacts in discrete element simulations [3,6–8,10,11,17,18]. Each model represents particular physical phenomena at the origin of contact cohesion such as solid surface adhesion, capillarity, cementation, and sintering.

Details of the contact cohesion model used for the present studies can be found in [11]. This model assumes an elastic-brittle behavior with a yield function that was extracted from experiments. The elastic behavior is characterized by three stiffnesses E_n, E_t and E_γ, so that $f_n=E_n d_n$, $f_t=E_t d_t$, and $M=E_\gamma \gamma$. As usual, damping actions are added in order to account for contact inelasticity and ensure numerical stability.

This elastic behavior holds as long as the contact actions remain below a "yield surface" $\zeta=\zeta(f_n,f_t,M)=0$. We used the following function that fits our previous experimental tests where a particular type of glue was employed to stick cylindrical particles together [11]:

$$\zeta=\left(\frac{f_n}{f_n^y}\right)+\left(\frac{f_t}{f_t^y}\right)^2+\left(\frac{M}{M^y}\right)^2-1, \tag{1}$$

where f_n^y, f_t^y, and M^y are the yield parameters for normal, tangential, and angular actions, respectively. The elastic do-

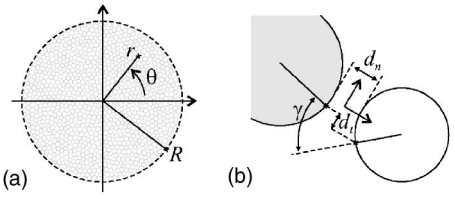

FIG. 1. (a) Geometry of the sample; (b) relative displacements between two edge points belonging to two particles and coinciding initially with their contact point.

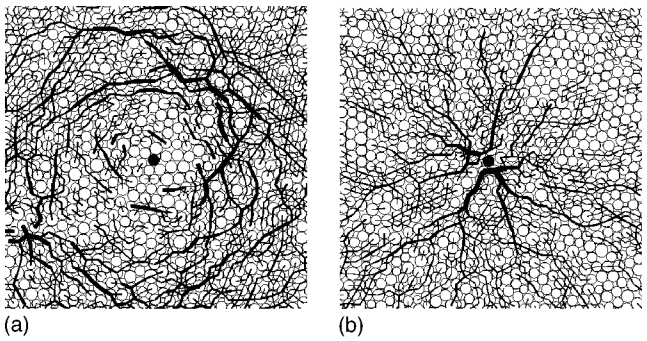

FIG. 2. Tensile (a) and compressive (b) normal forces generated by the swelling of a single particle (in black). The linewidth is proportional to the normal force.

main corresponds to $\zeta<0$. Note that f_n can take indefinitely large values (the positive sign corresponding to compressive forces) but it has a lower bound $f_n=-f_n^y$ that defines the largest tensile force that can be sustained by a contact. As soon as $\zeta\geqslant 0$, the cohesive bond breaks down irreversibly and the contact turns into noncohesive frictional behavior [19].

The shape of the yield function ζ and the values of the parameters will naturally influence the failure properties of the material as a whole for a specified loading mode. In our system, loading by particle swelling or shrinkage with a radial gradient induces appreciable displacements only along the contact normals. Using different values of f_t^y and M^y does not influence the results that will be discussed below. In other words, the failure is governed by extensional strain when f_n^y is reached at a strongly tensile contact in the sample.

On the other hand, as we shall see below, the sample-scale displacements in the elastic range are mainly controlled by the rate of particle size change, so that the behavior is not sensitive to the choice of the elastic parameters E_n, E_t, and E_γ. These remarks apply only to the loading mode and boundary conditions that we employed for the present investigation (in order to be able to get explicit analytical solutions). It is obvious that the situation would be different if more complex loading or anisotropic boundary conditions were used instead.

We used samples composed of 1133 polydisperse disks with a uniform distribution of diameters D within a range $[D_{\min},D_{\max}]$ where $D_{\max}=1.2\,D_{\min}$. The coefficient of friction is $\mu=0.1$. Each sample is created by removing all particles belonging to a noncohesive assembly in static equilibrium except those contained inside a circle of radius R_0. The cohesive bonds are then switched on and the sample is allowed to relax to equilibrium. The samples prepared by this procedure correspond to a dense but disordered packing of solid fraction $\simeq 0.89$ and coordination number 3.8.

The initial configuration is set as the reference state for our system so that the contact actions are identically zero everywhere. Obviously, multiplying all particle diameters by the same factor does not disturb this state since no relative motions are generated at the contact points, whereas *differential* particle-size change gives rise immediately to permanent compressive and tensile force gradients. For instance, the swelling of a single particle produces compressive radial forces by pushing the neighboring particles outward, as well as tensile orthoradial forces by increasing the total length of the "rings" of contiguous particles surrounding the swelling particle; see Fig. 2. A slight shrinkage of the same particle produces exactly the same force patterns with the signs inverted everywhere (compressive contacts turning to tensile, and vice versa).

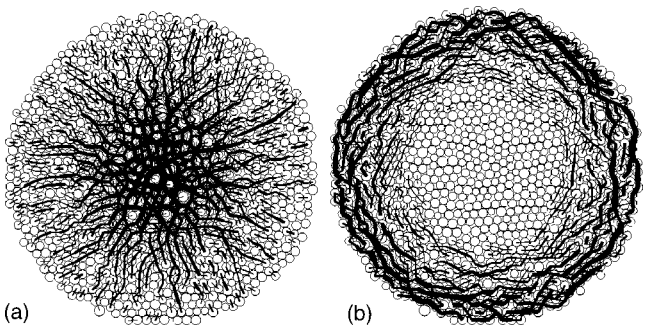

FIG. 3. Compressive (a) and tensile (b) forces in a shrinkage simulation.

Since we are interested here only in the effect of bulk straining, we require that the swelling rate $\dot{s}_i\equiv\dot{D}_i/D_i$ of each particle i be independent of its diameter D_i. We use the simplest swelling kinetics defined by a constant gradient from the center to the edge, $\dot{s}_i=(\alpha/R_0)r_i$, where r_i is the distance of the particle to the system center and α is a constant rate. Positive and negative values of α correspond to particle swelling and shrinkage, respectively.

Figure 3 shows snapshots of normal compressive and tensile forces in a shrinkage simulation. Although at the very local scale the forces are inhomogeneously distributed, we observe radial and orthoradial compressive forces decreasing in magnitude from the center to the edge, as well as orthoradial tensile forces decreasing in magnitude from the edge to the center. The cracks appear on the edge as soon as the first tensile contact fails, and they propagate toward the center as shown in Fig. 4(b). In swelling simulations, the respective roles of compressive and tensile roles are simply interchanged with respect to the shrinkage case. As a result, the cracks are initiated at the center, and they propagate toward the edge; see Fig. 4(a).

The coarse-grained stresses can be evaluated from the contact forces by means of the "micromechanical" expression of the stress tensor $\boldsymbol{\sigma}$ [20],

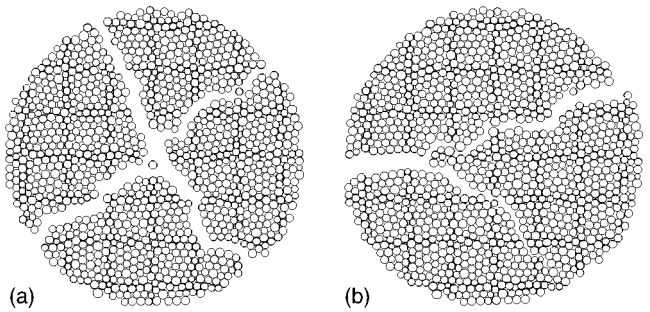

FIG. 4. Crack patterns in swelling (a) and shrinkage (b) simulations.

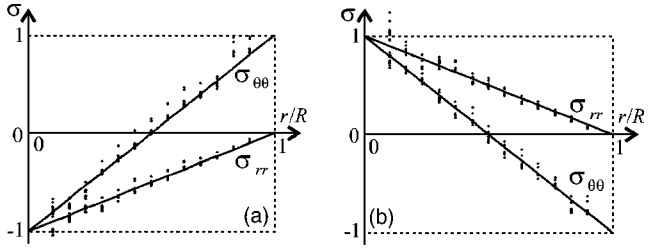

FIG. 5. Normalized stress components as a function of distance r to the center in swelling (a) and shrinkage (b) simulations. The full lines are elastic fits.

$$\sigma_{ij} = \frac{1}{V}\sum_{c\in V} f_i^c \ell_j^c, \tag{2}$$

where i and j design the coordinates, V is the control volume over which the stress tensor is evaluated (the contacts c taken from this volume), f_i^c is the i component of the force $\boldsymbol{f}^c$ at contact c, and ℓ_j^c is the j component of the vector $\boldsymbol{\ell}^c$ joining the centers of the two contact neighbors.

The stress tensor is a well-defined average if the control volume V contains a sufficiently large number of contacts. This requirement is satisfied by taking concentric circular volume elements as suggested by the rotational invariance of our system. We use polar coordinates and the radial and angular positions will be denoted by r and θ, respectively; see Fig. 1(a). As a result of isotropic straining, the cross components $\sigma_{r\theta}$ are zero.

The radial stress σ_{rr} and orthoradial stress $\sigma_{\theta\theta}$ are shown in Fig. 5(a) as a function of distance r to the center at different stages of a swelling simulation. For each data set at a given instant of evolution, we have normalized the distance r by R and the stress components by the largest tensile stress $-\sigma_{\max}$ (occurring at the center). We see that the normalized stresses collapse on a straight line as a function of r and they agree nicely with a one-parameter analytical fit that will be detailed below. Note that σ_{rr} is negative (tensile stress) throughout the sample, whereas $\sigma_{\theta\theta}$ changes sign at $r \simeq R/2$. In the case of shrinkage simulations, similar results are obtained with opposite signs, as shown in Fig. 5(b).

We now turn to analytical evaluation of the stresses. At a coarse-grained scale, the granular assembly will be represented by a linear elastic medium with an effective stiffness E and an effective Poisson's ratio ν. This is a plausible assumption, although, as we shall see below, the behavior of the stresses as a function of r is independent of the nature of the interactions. On the other hand, coarse-grained swelling at a point A of polar coordinates (r,θ) in space is equivalent to an imposed isotropic *space dilation* $\dot{s}(r,\theta)=\langle \dot{s}_i\rangle_{i\in V(r,\theta)}$, where the average is taken over all particles contained in a representative volume $V(r,\theta)$ centered on A. Since the rates are independent of particle diameters, we get

$$\dot{s} = \frac{\alpha}{R_0} r. \tag{3}$$

Then, the strain-rate tensor $\dot{\boldsymbol{\varepsilon}}$ at a point is the sum of two terms,

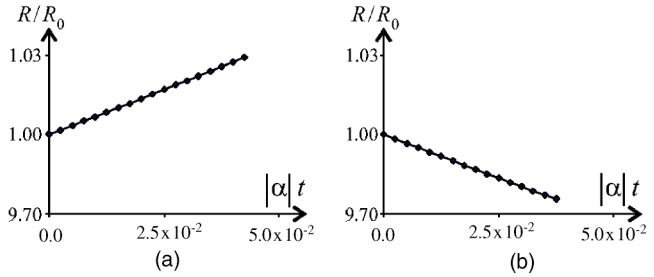

FIG. 6. Evolution of the sample radius R in swelling (a) and shrinkage (b) simulations.

$$\dot{\boldsymbol{\varepsilon}} = \dot{\boldsymbol{\varepsilon}}^e + \dot{s}\boldsymbol{I}, \tag{4}$$

where $\dot{\boldsymbol{\varepsilon}}^e$ is the elastic strain rate, $\boldsymbol{I}$ represents the unit tensor, and $\dot{s}\boldsymbol{I}$ is the metric change rate.

We assume that the displacement field $\boldsymbol{u}(r,\theta)$ is radial [according to the symmetry of straining expressed by Eq. (3) and that of the sample] so that $\dot{\varepsilon}_{r\theta}\equiv 0$. Since the radius R of the sample changes with time, Hooke's laws will be written in the form of rate equations,

$$\dot{\varepsilon}_{rr}^e = \dot{\varepsilon}_{rr} - \dot{s} = -\frac{1}{E}(\dot{\sigma}_{rr} - \nu\dot{\sigma}_{\theta\theta}),$$

$$\dot{\varepsilon}_{\theta\theta}^e = \dot{\varepsilon}_{\theta\theta} - \dot{s} = -\frac{1}{E}(\dot{\sigma}_{\theta\theta} - \nu\dot{\sigma}_{rr}), \tag{5}$$

where extensional strains and compressive stresses are counted positive. We need also the balance equation, which takes the following form in polar coordinates:

$$\dot{\sigma}_{\theta\theta} - \dot{\sigma}_{rr} = r\frac{\partial\dot{\sigma}_{rr}}{\partial r}. \tag{6}$$

The set of equations (3), (5), and (6) is easily integrated over time and space using the boundary conditions $\boldsymbol{u}(r=0)=0$ (imposed by 3) and $\sigma_{rr}(r=R)=0$ (by continuity of the normal stress at the boundary). The solution is

$$R = \frac{R_0}{1-2\alpha t/3},$$

$$\sigma_{rr} = E\left(1-\frac{R_0}{R}\right)\left(\frac{r}{R}-1\right),$$

$$\sigma_{\theta\theta} = E\left(1-\frac{R_0}{R}\right)\left(2\frac{r}{R}-1\right). \tag{7}$$

We see that both stress components are linear in r. The simulation data of Fig. 5 were fitted by adjusting only the effective elastic modulus E. The evolution of the system is, however, nonlinear as a function of time. The evolution of R is shown in Fig. 6 for swelling ($\alpha>0$) and shrinkage ($\alpha<0$) simulations together with the analytical fit from Eq. (7) which involves no fitting parameter. The agreement is excellent although the nonlinear nature of the evolution cannot be seen for $|\alpha|t \ll 1$. The largest tensile stress $\sigma_{\max}$ occurs on the edge for shrinkage and at the center for swelling. From Eq.

(7), we get $\sigma_{\max}=\frac{2}{3}E|\alpha|t$. Again, this linear form nicely fits the evolution of $\sigma_{\max}$ (by virtue of the fits shown in Fig. 5) up to failure for $\sigma_{\max}=\sigma^y$. The latter represents the effective tensile strength of the material.

It is worth noting that Poisson's ratio ν does not appear in Eqs. (7) and the only role of the stiffness E is to set the stress scale. This means that the behavior of the stress components and sample size as a function of r is independent of the local force law. In particular, in the limit of infinitely rigid particles, the same results remain true up to a stress scale which may be fixed through a confining pressure. More generally, both the local interactions and the mass or heat transfer influence the stress scale.

By analogy with molecular solids, we introduce a "theoretical" tensile strength σ^y_{theor} based on the interactions between two particles [13]. According to Eq. (2), the orthoradial stress is

$$\sigma_{\theta\theta}=n_c\langle f_\theta \ell_\theta\rangle \simeq n_c\langle\ell\rangle\langle f_\theta\rangle, \tag{8}$$

where n_c is the number density of contacts and $\langle\cdots\rangle$ designs averaging over the control volume. The largest value of $\sigma_{\theta\theta}$ in tension corresponds to the limit where all forces are polarized in the same direction and they have all reached the largest tensile force f_n^y. This defines a "theoretical" tensile strength

$$\sigma^y_{\text{theor}}=n_c\langle\ell\rangle f_n^y. \tag{9}$$

In our simulations, the measured tensile strength σ^y is below σ^y_{theor} by a factor $\simeq 4.3$. In molecular solids, a similar discrepancy between σ^y_{theor}, defined from atomic interactions in a regular atomic arrangement, and σ^y stems from "built-in" disorder (defects, damage) at different scales leading to stress concentration. In a granular solid, the disorder is "intrinsic" to the structure. As a result, the contact forces both in cohesive and noncohesive granular media have a wide distribution with a decreasing exponential shape for strong forces [8,15]. In fact, σ^y_{theor} reflects the *strongest* contact force at failure, whereas σ^y represents the *mean* tensile force by construction. Indeed, the simulations show that the ratio of the largest tensile force (at the contact where failure is initiated) to the mean tensile force [which is proportional to the mean stress according to Eq. (8)] is of the order of $\sigma^y_{\text{theor}}/\sigma^y \simeq 4.3$.

As far as we know, this is the first example showing how the local force inhomogeneities in a granular material control a macroscopic property, namely the tensile strength. Further investigations are, however, necessary in order to assess in more detail this correlation between the distribution of contact forces and the tensile strength. The shape of the probability density functions of contact forces is quite robust with respect to system parameters and the specific features of the contact force model. Nevertheless, the range of tensile forces varies as a function of adhesion, compactness, and probably some other details of the packing structure such as its anisotropy. Hence, we expect that the ratio between the theoretical and effective tensile strengths should reflect mostly those parameters pertaining to the granular structure rather than the contact force model.

Let us also underline here the brittle nature of our system that allows the first contact failure to propagate rapidly throughout the packing. For an elastoplastic contact model, particle rearrangements might take place and dissipate efficiently elastic energy. In this case, the packing undergoes a cumulative damage and the tensile strength will not be controlled only by the strongest tensile contacts.

In summary, our numerical data and their comparison with an analytical evaluation of stresses in the elastic domain and at failure suggest that a macroscopically elastic behavior is relevant up to crack initiation, as in molecular solids. However, the tensile strength is dependent on the inhomogeneous transmission of forces. The simple test described in this paper not only provides reproducible results, but it has also the advantage of combining features of discrete modeling with theoretical predictability at the macroscopic scale.

This approach may now be used to investigate and to predict the tensile thresholds and crack propagation in cohesive granular materials as a function of the initial density and anisotropy of the material or the possible couplings of the local cohesion with mass and heat transfer in the pores as in fine soils and granular rocks [21]. The theoretical approach can be extended to other structured media involving mesoscopic length scales, such as gels [22], cellular media [23], layered structures such as wood [24], and pastes [25]. Swelling or shrinkage may occur as a result of cellular growth (in biological systems) or the evolution of local variables such as water content and temperature.

It is a pleasure to thank J.-C. Bénet and J. N. Roux for helpful suggestions.

[1] D. Maugis, *Contact, Adhesion and Rupture of Elastic Solids* (Springer, Berlin, 1999).
[2] J. K. Mitchell, *Fundamentals of Soil Behavior* (Wiley, New York, 1993).
[3] C. Thornton and K. K. Yin, Powder Technol. **65**, 153 (1991).
[4] C. Thornton and S. J. Antony, Powder Technol. **109**, 179 (2000).
[5] T.-H. Kim and C. Hwang, Eng. Geol. (Amsterdam) **69**, 233 (2003).
[6] S. Luding, K. Manetsberger, and J. Müllers, J. Mech. Phys. Solids **53**, 455 (2005).
[7] M. Oda and K. Iwashita, Int. J. Eng. Sci. **38**, 1713 (2000).
[8] F. Radjai, I. Preechawuttipong, and R. Peyroux, in *Continuous and Discontinuous Modelling of Cohesive Frictional Materials*, edited by P. Vermeer, S. Diebels, W. Ehlers, H. Herrmann, S. Luding, and E. Ramm (Springer-Verlag, Berlin, 2001), pp. 148–159.
[9] J.-Y. Delenne, M. S. E. Youssoufi, and J.-C. Bénet, C. R. Mec. **330**, 475 (2002).
[10] S. Luding, R. Tykhoniuk, and J. Tomas, Chem. Eng. Technol.

26, 1229 (2003).
[11] J.-Y. Delenne, M. S. E. Youssoufi, F. Cherblanc, and J.-C. Bénet, Int. J. Numer. Analyt. Meth. Geomech. **28**, 1577 (2004).
[12] H. M. Jaeger, S. R. Nagel, and R. P. Behringer, Rev. Mod. Phys. **68**, 1259 (1996).
[13] *Statistical Models for Fracture in Disordered Media*, edited by H. J. Herrmann and S. Roux (North Holland, Amsterdam, 1990).
[14] D. M. Mueth, H. M. Jaeger, and S. R. Nagel, Phys. Rev. E **57**, 3164 (1998).
[15] F. Radjai, D. E. Wolf, M. Jean, and J.-J. Moreau, Phys. Rev. Lett. **80**, 61 (1998).
[16] M. P. Allen and D. J. Tildesley, *Computer Simulation of Liquids* (Oxford University Press, Oxford, 1987).
[17] T. Mikami, H. Kamiya, and M. Horio, Chem. Eng. Sci. **53**, 1927 (1998).
[18] G. A. D'Addetta, F. Kun, and E. Ramm, Granular Matter **4**, 77 (2002).
[19] S. Luding, in *Physics of Dry Granular Media*, Vol. 350 of NATO Advanced Study Institute Series E: Applied Sciences, edited by H. J. Herrmann, J.-P. Hovi, and S. Luding (Kluwer Academic Publishers, Dordrecht, 1998), pp. 285–304.
[20] J. Christoffersen, M. M. Mehrabadi, and S. Nemat-Nasser, J. Appl. Mech. **48**, 339 (1981).
[21] E. J. Tarbuck and F. K. Lutgens, *Earth: An Introduction to Physical Geology* (Pearson Education, Inc., New Jersey, 2002).
[22] I. Mrani, J.-C. Bénet, and G. Fras, Appl. Mech. Rev. **48**, 717 (1995).
[23] U. S. Schwarz and S. A. Safran, Phys. Rev. Lett. **88**, 048102 (2002).
[24] H. Kübler, For. Prod. Abstracts **10**, 61 (1987).
[25] G. Ponsart, J. Vasseur, J. M. Frias, A. Duquenoy, and J. Méot, J. Food. Eng. **57**, 277 (2003).